Check for updates

View Article Online
View Journal

PCCP

Accepted Manuscript

This article can be cited before page numbers have been issued, to do this please use: J. G. GARCIA OVEJERO, I. Morales, P. la Presa, N. Mille, J. Carrey, M. Garcia, A. Hernando and P. Herrasti, *Phys. Chem. Chem. Phys.*, 2018, DOI: 10.1039/C8CP02513D.

This is an Accepted Manuscript, which has been through the Royal Society of Chemistry peer review process and has been accepted for publication.

Accepted Manuscripts are published online shortly after acceptance, before technical editing, formatting and proof reading. Using this free service, authors can make their results available to the community, in citable form, before we publish the edited article. We will replace this Accepted Manuscript with the edited and formatted Advance Article as soon as it is available.

You can find more information about Accepted Manuscripts in the author guidelines.

Please note that technical editing may introduce minor changes to the text and/or graphics, which may alter content. The journal's standard Terms & Conditions and the ethical guidelines, outlined in our author and reviewer resource centre, still apply. In no event shall the Royal Society of Chemistry be held responsible for any errors or omissions in this Accepted Manuscript or any consequences arising from the use of any information it contains.

ROYAL SOCIETY OF CHEMISTRY

rsc.li/pccp

Journal Name

View Article Online
DOI: 10.1039/C8CP02513D

ARTICLE

Hybrid nanoparticles for magnetic and plasmonic hyperthermia

Jesus G. Ovejero*[a,b], Irene Morales[a,b], Patricia de la Presa[a,b], Nicolas Mille[c,d], Julian Carrey[c,d]

Miguel A. Garcia[a,b], Antonio Hernando[a,b] and Pilar Herrasti[e]

Received 00th January 20xx,
Accepted 00th January 20xx

DOI: 10.1039/x0xx00000x

www.rsc.org/

The present manuscript studies the use of hybrid magneto-plasmonic nanoparticles (HMPNP) based on iron oxide nanoparticles and Au nanorods as colloidal nanoheaters. The individual synthesis of the magnetic and plasmonic components allowed to optimize their feature for heating performance separately, before they were hybridized. Besides, detailed characterizations and finite element simulations were carried out to explaine the interaction effects observed between the phases of the HMPNP. The study also analyzed the heating power of these nanostructures when were excited with infrared light and AC magnetic fields, and compared it with the heating power of their plasmonic and magnetic component. In the latter case, the AC magnetization curves revealed that the magnetic dipolar interactions increase the amount of heat released by the hybrid nanostructures.

Introduction

Inorganic nanoparticles (NPs) with active properties for heat dissipation, such as magnetic and plasmonic NPs, open the possibility of inducing a contactless and local heating. The heat released by these NPs can be employed in a plethora of technological applications such as cancer treatment[1], catalysis[2] or water purification[3]. One of the most interesting applications in the biomedical field is the so-called hyperthermia therapy. This technique treats local tumors by inducing a thermal shock in cancer cells that activates apoptotic death mechanisms[4,5]. The most popular modalities of hyperthermia treatments mediated by NPs are magnetic hyperthermia[6] and plasmonic photothermia[7].

In magnetic hyperthermia, the heat is produced by the hysteresis losses generated by magnetic NPs when are exposed to high frequency alternating magnetic fields. The magnetic nanoagents employed in this approach must present a superparamagnetic behavior at low frequency fields, high saturation magnetization and high magnetic susceptibility[6,8]. Iron oxide nanoparticles (IONPs) are the most widely employed material for this purpose due to their good magnetic features and their high biocompatibility with human cells[9].

A novel strategy proposed to enhance the heating power in magnetic hyperthermia consists on controlling the effect of dipolar interactions between the magnetic NPs[10,11]. It has been postulated that, in a linear arrangement of IONPs, the dipolar interactions modify the effective anisotropy field (H_K) of the aggregates and can increase the hysteresis losses of the system[10–12]. However, such increment can only be achieved if the maximum field applied (H_{MAX}) is larger than the H_K of the system[12,13]. Thus, the enhancement of heating performance via dipolar interactions demands a careful analysis of the ratio between the H_{MAX} and the H_K generated in each specific system[10].

On the other hand, the plasmonic photothermia take advantage of the heat generated by metallic nanoparticles when are irradiated with laser light. The electron oscillation induced by the electric field of the laser, known as localized surface plasmon, derives in the generation of phonons in the atomic lattice that are eventually dissipated to the media as heat[14]. Au NPs, and most specially Au nanorods (AuNRs)[15], present excellent plasmonic properties for tailoring their optical spectra in the visible and infrared (IR) range maximizing their light absorption[16] and heat generation in deep tissues[17].

Recently, it has been observed that, using the appropriate NPs, these two approaches can be combined[18]. The large amount of heat dissipated by such magneto-plasmonic approach can help to enhance the effectivity of the in vivo treatment reducing the amount of nanoparticles and radiation dose required for the therapy[19]. Besides, the combination of magnetic and plasmonic components brings new biomedical possibilities such as theragnostic approaches[20,21] and magnetically enhance treatments[22]. However, there is still a lack of biocompatible materials that combine suitable magnetic and plasmonic properties to be use for this purpose.

Hybrid magneto-plasmonic nanoparticles (HMPNP) have been developed to address the issue combining magnetic and metallic phases in a single nanostructure. However, in this kind of nanostructures, the interactions between the phases can compromise the magnetic and plasmonic responses. An interesting strategy to address this issue consist in introducing a third biocompatible material (polymers, inorganic materials, etc.) that acts as spacer[23] and avoids common interfaces between them. Silica (SiO_2) has outstand over other alternatives due to its high thermal, mechanical and chemical stability[24,25].

[a] Instituto de Magnetismo Aplicado, 'Salvador Velayos', UCM-CSIC-ADIF, Las Rozas, PO Box 155, Madrid 28230, Spain.
[b] Departamento Física de Materiales, Facultad Ciencias Físicas, Universidad Complutense de Madrid, 28040 Madrid, Spain.
[c] Laboratoire de Physique et Chimie des Nano-Objets (LPCNO), Université de Toulouse, INSA, UPS, F-31077 Toulouse, France.
[d] CNRS, UMR 5215, F-31077 Toulouse, France.
[e] Departamento de Química Física Aplicada, Facultad de Ciencias, Universidad Autónoma de Madrid, Cantoblanco s/n, 28049 Madrid, Spain
Electronic Supplementary Information (ESI) available: See DOI: 10.1039/x0xx00000x

Published on 24 August 2018. Downloaded by Freie Universitaet Berlin on 8/24/2018 4:31:16 PM.

Physical Chemistry Chemical Physics Accepted Manuscript

Please do not adjust margins

View Article Online
DOI: 10.1039/C8CP02513D

Published on 24 August 2018. Downloaded by Freie Universitaet Berlin on 8/24/2018 4:31:16 PM.

In this article, we explore the possibility of using recently developed HMPNPs in which IONPs and AuNRs are coupled with a silica shell[26], as magnetic and plasmonic nanoheaters. The HMPNP response at high frequency magnetic fields and IR laser excitation were studied in detail to analyze their heating power as well as the effect of the interaction between the different phases on the hybrid nanostructures.

Experimental

Reactants

Ethanol, hexadecyltrimethylammonium bromide (CTAB), chloroauric acid ($HAuCl_4$), sodium borohydride ($NaBH_4$), silver nitrate ($AgNO_3$), sodium hydroxide (NaOH), ascorbic acid, poly(ethylene glycol) thiol (PEG-SH) and tetraethyl orthosilicate (TEOS) were purchased from Sigma-Aldrich (www.sigmaaldrich.com). Ultrapure water, tetrabutylammonium bromide (TBAB) and ammonia (NH_3) were purchased from Panreac (www.panreac.es). Fe slides were purchased from GoodFellow (www.goodfellow.com). Citric acid was purchased from Merk (www.merck.es).

Synthesis of AuNR

AuNRs were synthesized using the seed-mediated growth method of El-Sayed et al[27]. Firstly, seeds were prepared using a solution of CTAB (5 mL, 0.1 M) and $HAuCl_4$(0.25 mL, 10 mM) gently mixed. 0.3 mL of 10 mM ice cooled $NaBH_4$ were added drop by drop to the solution and the mixture was allowed sitting for 1 hour in a thermostatic bath at 30 °C.

For AuNRs growth, 250 mL of CTAB solution 0.1 M were mixed with 12.45 mL of $HAuCl_4$ (10 mM) and 2 mL of $AgNO_3$ (10 mM). Au ions were reduced by adding ascorbic acid (1.2 mL, 0.1 M). AuNR with different aspect ratio (AR) were prepared by adding different amount of Au seeds solution to the growth solution: 30 µL (AR=3.15), 60 µL (AR=3.38), 120 µL (AR=3.86) and 240 µL (AR=4.38). The reaction mixture was sat overnight at 30 °C. The suspension of AuNRs was cleaned with water by triple centrifugation of 10000 rpm for 30 min.

AuNRs were concentrated to 0.8 mM (OD_{400nm}=2). 25 mg of SH-PEG (Mw=6000) were dissolved in 2.5 mL of water and introduced in an ultrasound (US) bath for 25 min to dissolve them. Then, 8.75 mL of AuNR and 2.32 mL of SH-PEG solution were mixed under gentle stirring for 6 h. After the pegylation, the samples were centrifugated at 10000 rpm for 30 min and the medium was progressively substituted by pure ethanol.

Synthesis of IONP

The electrochemical synthesis of IONPs was carried out oxidizing a metallic electrode in a conductive solution of tetrabutylammonium bromide 40 mM applying a current density of 45 mA cm^{-2} for 30 minutes. Two flat Fe plates of 2 cm^2 (electrode) and 8 cm^2 (counterelectrode) were faced with a 1 cm gap between them. The solution was mixed at 400 rpm using a magnetic stirrer. The reaction temperature was fixed to 5ºC using a thermostatic glass. After three magnetic decantation and cleaning, the IONPs were immediately coated with citric acid by adding 25 mL of 0.1 M citric acid to the NPs under stirring. After adjusting the pH to 5 using diluted NaOH, the dispersion was heated up to 80 °C for 2 h. Ferrite NPs were cleaned again by triple magnetic decantation.

Synthesis of hybrid AuNR-IONP

Hybrid (AuNR/IONP)@SiO_2 NPs were prepared using a modification of Stöber method[26,28]. Optical density of AuNRs was adjusted to 1 mM (OD_{400nm}=2.4) by adding pure ethanol and IONPs were suspended in water at a concentration of 0.7 g_{Fe} L^{-1}.

In a 12.5 mL plastic tube, 2.04 mL of IONP dispersion were added to 7 mL of AuNR in order to establish a solvent ratio of ethanol/water= 3.5. The mixture was shaken and sonicated for 5 min. The pH was risen to ~8.5 adding 0.04 mL of NH_3 (28%). Then, 2.04 mL of TEOS were added and the dispersion was shaken and sonicated for other 5 min. Thereafter, the mixture was placed in an ultrasound bath for 2 hours maintaining the temperature bellow 50 °C. The HMPNP produced were cleaned by triple centrifugation of 30 min at 3000 rpm. Supernatant was discarded and the HMPNPs were stored in pure ethanol. For hyperthermia experiments the medium was substituted by water following a similar centrifugation process.

Characterization

Size and geometry of AuNRs, IONPs and HMPNPs were studied using a transmission electron microscopy (TEM) JEM-2100F (JEOL Ltd.). The average size of each collection of NPs was estimated measuring more than 150 NPs and fitting the data with a log-normal distribution. Colloidal features such as hydrodynamic diameter (D_H) and polydispersity index (PDI) were obtained by means of Dynamic Light Scattering (DLS) a Zetasizer Nano (Malvern) using the values of scattered light intensity (intensity mode). The X-ray difraction patterns were acquired using a PANalytical X'Pert Pro Multi-Purpose Diffractometer with a CuKa (λ = 0.15418 nm). Raman experiments were carried out in a confocal Raman microscope (Witec ALPHA 300RA) equiped with a Nd:YAG laser (532 nm) in p-polarization. Fe and Au concentration of IONP and HMPNP colloids were estimated by inductively coupled plasma optical emission spectroscopy (ICP-OES), digesting an aliquot of the sample in aqua regia and diluting to a known Mili-Q® water volume (18.2 MΩ·cm @ 25 °C).

The optical extinction spectra were recorded using a UV-Vis-IR spectrometer Perkin Elmer Precisely Lambda 35 with a quartz cuvette of 1 cm path length. Quasistatic magnetic response of IONPs and HMPNPs were measured using a MPMS Quantum Design SQUID magnetometer. For these measurements, two sample preparations were studied: i) powder samples were measured by means of gelatin capsules with the residue of lyophilized colloids compacted with cotton; ii) colloidal samples were measured by using homemade paraffin sealed containers of 50 µL. The magnetization value of the colloids was estimated using the Fe concentration obtained by ICP-OES.

Magnetization curves were obtained applying a maximum magnetic field of 3 T. The susceptibility dependence with temperature (ZFC-FC curves) was obtained by applying a magnetic field of 10 mT. To record thermoremanence curves (TMR), the sample was cooled down with an applied field of 10 mT that was switched off at low temperatures. Then, the remanent magnetization was recorded in the absence of field while increasing the temperature. High frequency magnetization curves of colloid samples (0.5mL, 2.8 gL^{-1}) were

Physical Chemistry Chemical Physics Accepted Manuscript

This journal is © The Royal Society of Chemistry 20xx

Please do not adjust margins

View Article Online
DOI: 10.1039/C8CP02515D

measured using a home-made magnetometer, described in details in ref. [29]. The set-up reaches a maximum field of 65 mT at 56 kHz.

Theoretical calculations

Mie-Gans theory was employed to study the optical properties of the HMPNPs[30]. **Equations 1-3** describe the extinction cross section of a metallic prolate spheroid (a=b≠c) with a permittivity ε= $\varepsilon_1 + i\varepsilon_2$, surrounded by a dielectric medium with a real permittivity ε_m:

$$\sigma_{ext} = \frac{\omega}{3c}\epsilon_m^{3/2} V \sum_{j=a}^{c} \frac{\left(\frac{1}{P_j^2}\right)\epsilon_2(\omega)}{\left[\epsilon_1(\omega)+\left(\frac{1-P_j}{P_j^2}\right)\epsilon_m(\omega)\right]^2+\epsilon_2(\omega)^2} \quad (1)$$

$$P_c = \frac{1-e^2}{e^2}\left[\frac{1}{2e}\ln\left(\frac{1+e}{1-e}\right)-1\right]; P_a = P_b = \frac{1-P_c}{2} \quad (2)$$

$$e = \left[1-\left(\frac{a}{c}\right)^2\right]^{1/2} \quad (3)$$

Where ω is the frequency of the incident light. The presence of magnetite nanoparticles in the silica shell was included in the equations by assuming an effective medium, in which ε_{eff} is the weighted average of the silica permittivity and magnetite permittivity, as shown in **Equation 4**:

$$\epsilon_{eff}(\omega) = \Phi \cdot \epsilon_{Fe3O4}(\omega) + (1-\Phi)\cdot \epsilon_{SiO2}(\omega) \quad (4)$$

Where **Φ** is the amount of magnetite in the volume of the silica shell.

The near field enhancement of these nanostructures was simulated using the commercial software package COMSOL Multiphysics® that employs finite element method (FEM) for the analysis of the plasmonic response[31]. The extinction spectrum was obtained from the electric field ($\vec{E}$) and electric vector ($\vec{D}$) using **Equations 5**:

$$\sigma_{abs} = \frac{2}{c_0\varepsilon_0 n|E_{inc}|^2}\int_V Real(\sigma \vec{E}\cdot\vec{E}^* - i\omega\vec{E}\cdot\vec{D}^*)dV \quad (5)$$

Reflected and scattered waves were cancelled using a spherical perfect matching layer technique. The geometry of the HMPNP was reproduced as a Au proloid with the dimensions obtained in TEM pictures, surrounded by 6 spheres of Fe_3O_4 inserted in a concentric proloid of silica.

Calorimetric measurements

The heating power of the NPs was evaluated registering the increment of temperature when irradiated with high frequency magnetic fields and laser. **Equations 6** was used to evaluate the Specific Absorption Rate (SAR) of the samples.

$$SAR = \frac{C_V}{[X]}\frac{\Delta T}{\Delta t} \quad \text{Equation 6}$$

Where C_V is the specific heat of water (4.186 kJ L^{-1} K^{-1}) and [X] is the concentration of the sample in g L^{-1}. In the case of magnetic hyperthermia, fields between 6-65 mT and a frequency of 100 kHz were applied to a total sample volume of 0.5 mL. The increase of the temperature as a function of time was measured with two fiber optic thermometers placed at slightly different heights inside the colloid, acquiring the mean value of both temperature measurements.

In laser irradiation experiments (photothermia), the samples were measured with a non-adiabatic crystal capillary of 0.8 mm using a volume of 50 **μ**L of colloidal NPs. This volume was irradiated using a 785 nm laser (LDM785, Thorlabs) of 20 mW focused to cover the whole diameter of the capillary. The fiber optic thermometer was inserted directly in the dispersion and carefully placed out of the laser spot.

Results and discussion

Synthesis of HMPNP

The TEM images of the IONPs and AuNRs employed in the synthesis of HMPNP are presented in TEM images of **Figure 1a** and **1c**, respectively. The electrochemical synthesis of IONPs produces quasi-spherical ferrite NPs with an average size of 12.0 nm and a size dispersion of 0.5 (**Figure S1**). **Figure 1b** shows that these IONPs present magnetization curves with a high saturation magnetization value (M_S= 79 Am^2kg^{-1}) and small coercivity (H_C) at room temperature if they are measured in a quasistatic regime (dc-field), what indicates a superparamagnetic behavior. X-ray diffraction patterns and Raman spectrum (**Figure S4**) indicate that the magnetic phase of IONP is mainly magnetite (Fe_3O_4) although a small fraction of maghemite (γ-Fe_2O_3) could be present as well.

On the other hand, the synthesis of AuNRs by the method of El-sayed produces a monodisperse population of NPs in which transversal and longitudinal sizes can be tailored adjusting the amount of seed employed in the synthesis (**SI: Figure S2**). **Figure 1d** shows the extinction spectrum of the samples prepared adjusting the aspect ratio (AR) to 3.15, 3.38, 3.86 and 4.38. Changing the AR of the AuNRs, it was possible to modify the frequency of the longitudinal plasmon resonance. The IR absorption peak (associated to longitudinal plasmon) shifts to higher wavelengths as long as the AR of the AuNRs grows, what opens the possibility of fitting the position of the peak to the wavelength of the excitation laser.

HMPNP presented in **Figure 1e** were prepared functionalizing the IONPs and AuNRs with PEG and CA molecules respectively. Previous studies[26,32] showed that these two molecules bind each-other during the growth of silica coating and produces hybrid nanostructures with a core@satellites arrangement. In these nanostructures, the silica shell acts as a matrix that holds the magnetic and plasmonic component in a robust and chemically stable structure[23]. **Figure 1g** shows that silica shell grows between IONPs and the AuNR avoiding common interfaces of these two phases. Consequently, the interplanar distances registered in their closer surfaces results similar to their corresponding bulk materials in (111) and (220) crystalline directions. The X-ray diffraction patterns of HMPNPs confirmed that the interatomic distances of the individual components were preserved after the hybridization (**SI: Figure S4**). In spite of this, the short-distance interactions between the different phases of the hybrid nanostructure can modify the magnetic and plasmonic properties of the components.

Published on 24 August 2018. Downloaded by Freie Universitaet Berlin on 8/24/2018 4:31:16 PM.

Physical Chemistry Chemical Physics Accepted Manuscript

Please do not adjust margins

View Article Online
DOI: 10.1039/C8CP02517D

Published on 24 August 2018. Downloaded by Freie Universitaet Berlin on 8/24/2018 4:31:16 PM.

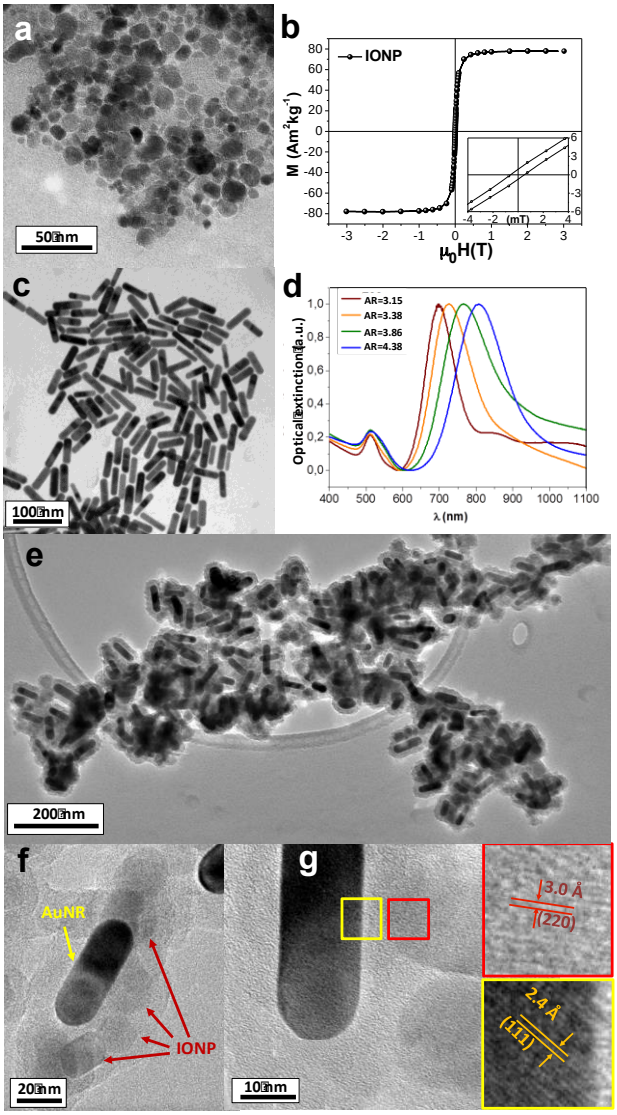

Figure 1. TEM images of: (a) iron oxide nanoparticles (IONP), (c) Au nanorods (AuNR) and (e, f) hybrid magneto-plasmonic nanoparticles (HMPNP). (g) HRTEM picture of HMPNP shows the atomic planes of IONP (upper inset) and AuNR (lower inset) in proximal sufaces. (b) Magnetization curve of IONPs at 300K measured in powder. (d) Normalized absorption spectra of Au nanorods with different AR: AR=3.15 (red), AR=3.38 (yellow), AR=3.86 (green) y AR=4.38 (blue).

Magnetic properties of IONP and HMPNP

Figure 2 shows the magnetization curves of IONPs and HMPNPs prepared as powders and colloids. It can be observed that the M_S of HMPNPs is drastically reduced to 17 A m^2 kg^{-1} as a consequence of the non-ferromagnetic phases present in the sample (Au and SiO_2). The insets of these figures show the first and second quadrant of normalized curves (dashed lines have been included as eye-guide). Comparing curves of powder preparation (black curves) of both systems, it is possible to observe that the HMPNP curves presents larger χ and higher H_C.

The direct interaction between Fe_3O_4 and Au phases is avoided by the silica interphase, which acts as a insulator spacer blocking the charge transference between them. Thus, in the study of the magnetic properties, the most relevant difference between both systems is the distance among magnetic NPs. In powder preparation, the IONPs are in close proximity to one another, while in HMPNPs, the silica coating increases the distance between IONPs and the shape of the AuNR favors their linear arrangement around the Au nucleus[26]. These two conditions modify substantially the effect of dipolar interactions in each case.

Using Monte-Carlo simulations, Serantes et al. observed that dipolar interactions can increase or reduce the effective H_K of a collection of magnetic NPs depending on their relative disposition[10]. In a linear arrangement, the effective H_K of the system is increased and their magnetization curve presents higher χ and H_C. On the contrary, for more compact arrangements (cubic, hexagonal, etc.), the dipolar interactions produce the opposite effect on the magnetic response. In the case of the HMPNPs, the presence of a Au nucleus prevents adjacent positions between IONPs and favors the linear arrangements of the IONP (**Figure S3**), what explains the higher H_C and χ observed for hysteresis loops of HMPNP measured as powder.

On the other hand, both systems present magnetization curves with larger χ and smaller H_C in liquid phase (red curves) respect to powder preparations (black curves). This effect can be attributed to the possibility of the particles to rotate freely in the liquid and align their easy magnetization axes with the field, increasing the magnetic susceptibility of the system.

In order to analyze further this effect, the zero field cooled (ZFC), field cooled (FC) and thermoremanence (TMR) curves were obtained for liquid phase preparation of both systems, as presented in **Figures 3**. It can be observed that in ZFC and FC curves the magnetization grows drastically at the melting temperature of water (273 K), and in TMR curves drop to nearly zero values. It can also be observed that in the case of HMPNPs, the curves change more progressively with temperature.

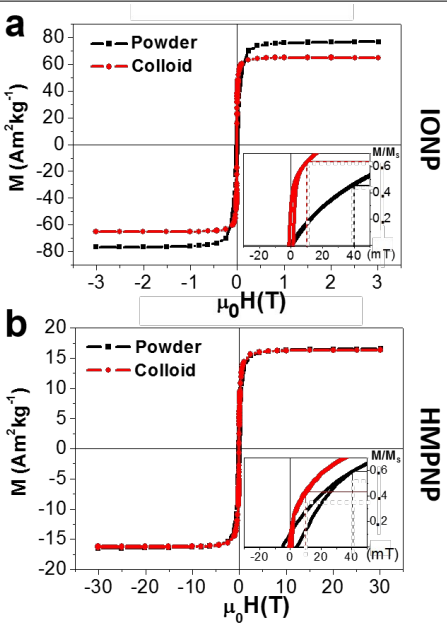

Figure 2. Magnetic hysteresis curves at 300 K of (a) IONP and (b) HMPNP. The insets present the normalized curves in which dash lines have been included as eye-guides. Both samples were measured as a powder (black) and as a colloidal suspension (red).

Physical Chemistry Chemical Physics Accepted Manuscript

This journal is © The Royal Society of Chemistry 20xx

Please do not adjust margins

View Article Online
DOI: 10.1039/C8CP02517D

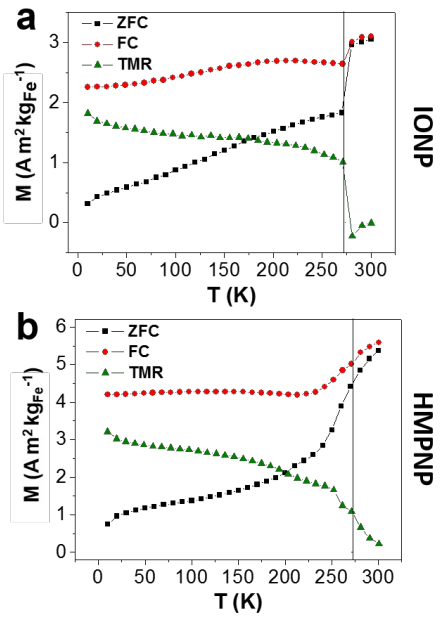

Figure 3. Zero Field Cooled (black squares), Field Cooled (red dots) and thermoremanence (green triangles) curves for (a) IONP and (b) HMPNP in liquid phase. Vertical line indicates the fusion temperature of water (273K).

When the dispersing media melts, the NPs are unblocked and the torque generated by the magnetic field can make them rotate, which increases the magnetization of the system. However, the HMPNPs comprise several IONPs with different magnetization easy axis and thus the torque generated by the magnetic field is not uniform in the whole nanostructure. In this kind of superparamagnetic systems, the effective torque induced by the field is divided by $\sqrt{N}$,[33] where N is the number of NPs contained in the agglomerates (~6 in this case, details in SI). Besides, the DLS measurements indicated that hydrodynamic diameter is significantly higher for HMPNPs (D_H =266 nm, PDI=0.20) than IONPs (D_H= 57 nm, PDI=0.17), which also hampers their Brownian rotation in a viscous media and hinders the magnetization process. This effects explain the higher susceptibility observed in the hysteresis loops of IONP in liquid phase.

Plasmonic properties of HMPNP

Figure 4a shows the optical extinction spectra measured for AuNR, silica coated AuNR (AuNR@SiO_2) and HMPNP samples. As it can be observed in AuNR@SiO_2, the longitudinal plasmon resonance shifts to higher wavelengths and becomes wider when the AuNRs are surrounded by dielectric media of higher permittivity such as silica ($\varepsilon_r \sim 2.1$). The shifting and widening of the peak become more significant in the case of HMPNP. **Figure 4b** compares the experimental spectrum of HMPNPs with the one predicted by Mie-Gans theory when assuming a 9% of magnetite in the surrounding media. It can be observed that although the position of both peaks matches, the width at half maximum registered for the longitudinal peak results much larger than the theoretical prediction (**Table 1**).

FEM simulations were carried out to analyze the discrepancies between experimental data and Mie-Gans spectrum. **Figure 4d** displays the geometry designed for the simulation of HMPNP plasmonic response. It is composed by a single Au proloid (a=51.9 nm, b=c=13.7 nm) surrounded by a silica shell 15 nm thick in which 6 Fe_3O_4 spheres of = 12 nm were randomly inserted (see details and other geometries in SI). The experimental permittivity values of Au[34], Fe_3O_4[35] and SiO_2[36] were implemented in the COMSOL Multiphysics simulations ad oc.

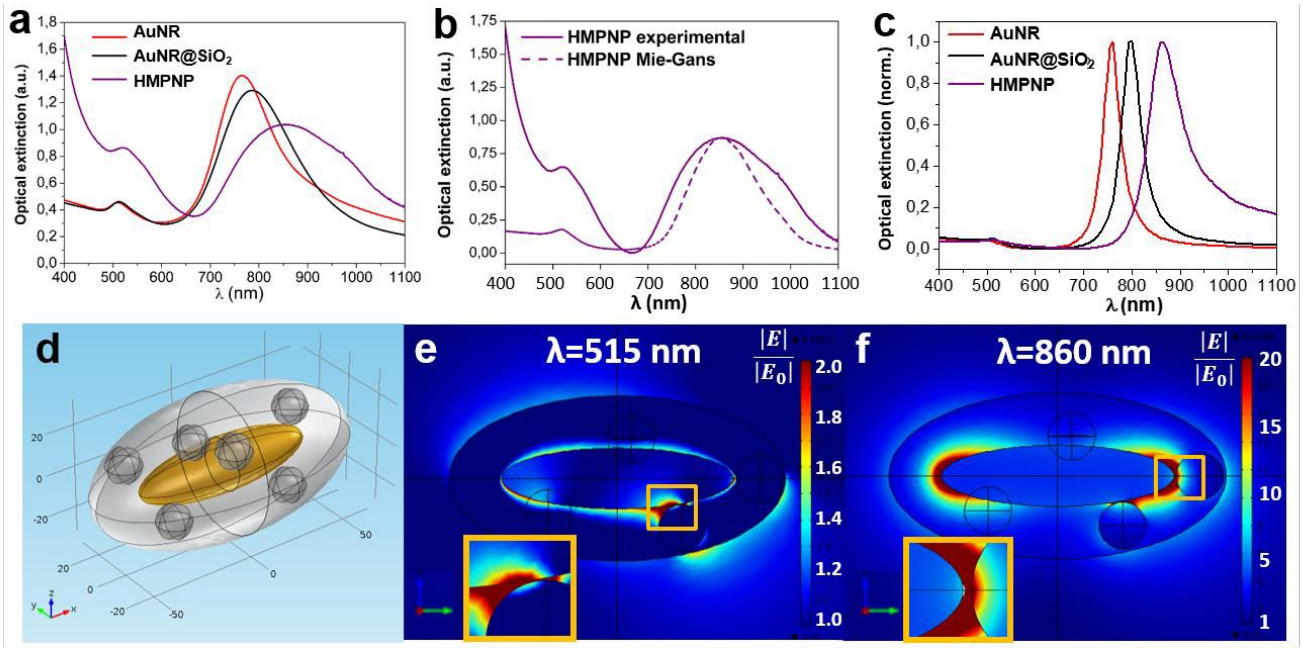

Figure 4. Plasmonic response of AuNR, AuNR@SiO_2 and HMPNP: (a) Experimental optical extinction spectra, (b) Comparative plot of experimental (continuous) and Mie-Gans theory (dash) extinction spectra of HMPNP, (c) Theoretical extinction spectra obtained by finite element method simulations (FEM). (d) Geometry used in FEM studies to simulate the plasmonic response of HMPNP. Near field enhancement generated at (e) transversal and (f) longitudinal plasmon resonances in the X-Z plane of HMPNP.

Published on 24 August 2018. Downloaded by Freie Universitaet Berlin on 8/24/2018 4:31:16 PM.

Physical Chemistry Chemical Physics Accepted Manuscript

Please do not adjust margins

View Article Online
DOI: 10.1039/C8CP02513D

	λ_{EXP} (nm)	$FWMH_{EXP}$ (nm)	λ_{MG} (nm)	$FWMH_{MG}$ (nm)	λ_{FEM} (nm)	$FWMH_{FEM}$ (nm)
AuNR	765	138	765	129	760	44
AuNR@SiO$_2$	785	165	782	151	790	50
HMPNP	857	261	860	195	861	86

Table 1. IR maximum wavelengths (λ) and full width at half maximum (FWHM) according to experimental data (EXP), Mie-Gans theory (MG) and finite element method simulations (FEM).

As shown in **Figure 4c**, the spectra obtained in AuNR, AuNR@SiO_2 and HMPNP simulations, reproduce the position of the longitudinal plasmon resonance peak (**Table 1**). However, the single nanoparticle simulations do not take into account the size dispersion of the samples, which generates much narrower absorption peaks. Despite that, the widening obtained for the longitudinal peak of an HMPNP respect to an uncoated AuNR resulted to be in good agreement with the one observed in experimental data (~1.9).

The patterns of electric field enhancement presented in **Figures 4e-f** for the transversal and longitudinal plasmon resonances of HMPNP explain this effect. In contrast to AuNR and AuNR@SiO_2 simulations (**SI:Figure S6**), the enhanced field around HMPNP does not follows to the radiation pattern of a dipolar antenna. The insets in these figures highlight the confinement of the electric field generated between IONP and AuNR surfaces. In appropriate conditions, such confinements increase the intensity of the plasmonic resonance and thus the amount of heat dissipated[37]. However, the disordered arrangement of the IONPs around the AuNRs produced by this synthesis method generates a heterogeneous polarization of the surrounding media that damps the IR extinction peak and explain the extra widening observed in the spectrum of HMPNP.

Magnetic hyperthermia in IONP and HMPNP

Figure 5 compares the magnetic response of IONPs and HMPNPs at high frequency. The high-frequency hysteresis curves in **Figure 5a** show that, at low H_{MAX}, the IONPs curves present an elliptical shape similar to the one predicted by linear response models[38]. According to these models, the magnetization of the sample varies linearly with the applied field and the delay between them determines curve parameters such as H_C or remanent magnetization. In this kind of cycles, the hysteresis area grows quadratically with H_{MAX}. When $\mu_0 H_{MAX}$ is over 29 mT, the magnetization starts to saturate and the curves do not present an elliptic shape anymore. This kind of curves needs to be explained using different approaches such as Stoner-Wohlfarth models[39].

The growth of the cycle area (A) with H_{MAX}^2 , presented in **Figure 5d**, shows also two regimes. When $\mu_0 H_{MAX}$ < 31 mT, the area of the cycle grows linearly respect to H_{MAX}^2 with a slope of 1.72 J g^{-1} T^{-2}, while at higher magnetic fields, the slope is reduced to 0.22 J g^{-1} T^{-2}. There is a linear relation between the area of the cycles and the power dissipated at a specific frequency. The corresponding SAR values were included in the right axis of the graph. They were calculated multiplying the area of the loops by the frequency of the excitation field ($\boldsymbol{\nu}$) (**Equation 7**).

$$SAR = A \cdot \nu \qquad \textbf{Equation 7}$$

In **Figure 5b**, the hysteresis curves of HMPNPs present a different dependence with H_{MAX}. At low fields, the curves are closed and thus magnetization reversal takes place without hysteresis. Only for $\mu_0 H_{MAX}$>23 mT it was possible to observe a significant area inside the curve. The growth of the area with H_{MAX}^2 in **Figure 5e** shows two regimes as well, with slopes of 1.34 J g^{-1} T^{-2} and 0.37 J g^{-1} T^{-2} for low and high fields respectively. In this case, the transition field between them is 42 mT.

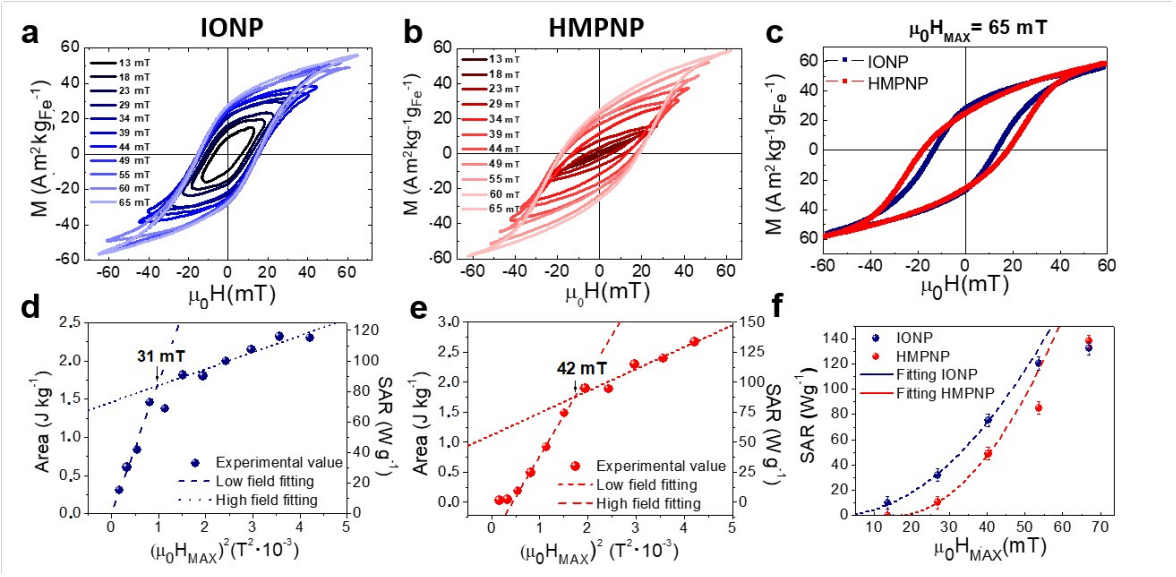

Figure 5. High frequency magnetic curves of (a) IONP and (b) HMPNP at different maximum fields (H_{MAX}). (c) Comparative graph of high frequency magnetic curves at $\mu_0 H_{MAX}$ = 65 mT. Dependence of the area with H_{MAX}^2 in magnetic curves of (d) IONP and (e) HMPNP. Dash and dot lines indicate the linear fittings of the data at low and high magnetic fields, respectively. The right axis indicates the corresponding SAR values. (f) Calorimetric measurements of SAR at different H_{MAX} for IONP and HMPNP. Dash line shows the quadratic fitting of the data at low fields.

Published on 24 August 2018. Downloaded by Freie Universitaet Berlin on 8/24/2018 4:31:16 PM.

Physical Chemistry Chemical Physics Accepted Manuscript

This journal is © The Royal Society of Chemistry 20xx

Please do not adjust margins

View Article Online
DOI: 10.1039/C8CP02513D

Published on 24 August 2018. Downloaded by Freie Universitaet Berlin on 8/24/2018 4:31:16 PM.

Such difference in transition fields can be related to the different effective H_K induced by dipolar interactions in IONPs and HMPNPs. According to Stoner-Wohlfarth theory, for a thermally blocked system of magnetic NPs with magnetization easy axis randomly oriented, the effective H_K of the system is 2.08 times the H_C of the curves[39]. In this way, H_K values were calculated from the H_C value of the loop measured at large magnetic field, obtaining 29 mT and 38 mT for IONP and HMPNP, respectively. In both cases, the transition between both regimes take place when H_{MAX} is close to 1.1 times the effective H_K of the system. According to numerical simulations of magnetic NP chains, the optimum H_{MAX} value permitting to maximize the area of the curves with respect to the field energy is approximately 1.1 times H_K[10]. These results indicate that the theoretical optimum value for H_{MAX} corresponds to the field at which the transition between the two growth regimes occurs.

On the other hand, comparing the maximum value of SAR in **Figure 5d** (SAR = 115 W g^{-1}) and **Figure 5e** (SAR = 134 W g^{-1}), it is possible to observe that HMPNPs are able to dissipate a larger amount of heat when the field is strong enough. **Figure 5c** presents together the hysteresis loops of IONP and HMPNP at the highest field (65 mT). It shows that, at this field, the HMPNPs generate loops with a higher H_C, which implies a larger area and thus larger SAR values. The H_C enhancement in HMPNPs agrees with the quasistatic curves of powder samples (**Figure 2b**).

Calorimetric measurements in **Figure 5f** are in good agreement with the conclusions extracted from high frequency loops. At low fields ($\mu_0 H_{MAX} \leq 40$ mT), the SAR of both samples grows quadratically with the field. The IONPs presents higher values of SAR in this range. However, when H_{MAX} is increased, the growth of SAR decays and HMPNPs overcomes IONPs. The enhancement of SAR values for IONPs in linear assemblies has been previously reported[11] and has also been associated with the effect of dipolar interactions.

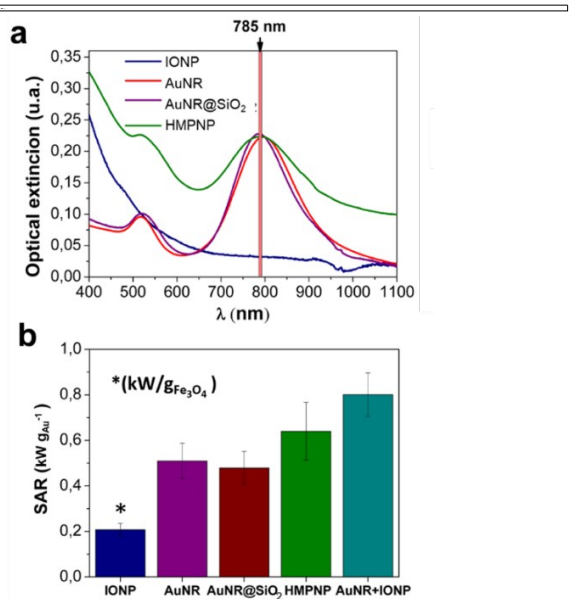

Figure 6. Extinction spectrum of IONP (blue), AuNR (purple), AuNR@SiO_2 (red) and HMPNP (green) samples used in photothermal assays. SAR values obtained for colloids of IONP, AuNR@CTAB, AuNR@SiO_2, HMPNP and a mixture colloid of AuNR@SiO_2 and IONP (turquoise).

Photothermia experiments

Figure 6a shows the extinction spectrum of the AuNR, AuNR@SiO_2 and HMPNP samples prepared for photothermal assays. The dash blue line displays the extinction spectra of IONPs employed in this study. The samples were prepared with AuNRs of different AR so that the maximum of the IR absorption peak matched with the wavelength of the excitation laser (**SI: Figure S7**). Besides, the number of NP was adjusted in each colloid to obtain similar optical extinction coefficient at 785 nm. In photothermal experiments, all the samples were irradiated with the maximum laser power accepted in human tissue (0.33 W cm^{-2}).

The SAR values obtained for different colloids are presented in **Figure 6b**. In order to be comparable, SAR values were obtained substituting in **Equation 7** the Au concentration of the colloids. Only in the case of IONPs the increment of temperature was divided by Fe_3O_4 concentration of the sample. It can be observed that although IONPs are not metallic and thus have not plasmonic response, they generate a certain amount of heat when are irradiated with an IR laser. To the best of our knowledge, the origin of this effect has not been fully explained yet[40,41], since at the wavelength employed, the absorption of Fe_3O_4 is minimum (**Figure 6a**). However, the heat produced by laser irradiation has been observed to be effective to enhance the hyperthermia performance of IONPs[19].

Comparing the SAR values of AuNR, AuNR@SiO_2 and HMPNP, it can be concluded that the presence of IONPs in the HMPNPs improves the photothermal performance of hybrid nanostructures. However, to distinguish the contribution of the different phases, an additional colloid of IONPs and AuNRs, with Au and Fe concentrations similar to HMPNP sample, was included in the study.

The turquoise column shows that this colloid presents the highest SAR value. The differences between this colloid and HMPNP should be associated to the interaction between AuNRs and IONPs observed in **Figure 4**. In this case the creation of inhomogeneous concentrations of electric field between the surfaces of both phases reduce the heating power of these kind of nanostructures. Further development of self-assembling techniques would be required to produce a cooperative interaction between plasmon resonance of AuNRs core and IONPs around them.

Conclusions

In this work Au nanorods and iron oxide nanoparticles were combined in a hybrid nanostructure by controlling the sol-gel silanization process. The resultant nanostructures present suitable magnetic and plasmonic properties for nanoheating purposes in biomedical applications. It has been observed that the hybrid samples display a larger coercive field, which induces larger heating at high magnetic fields than the IONPs. Besides, the heat generated by IONPs and AuNRs in photothermal heating can be combined using HMPNPs. However, it was observed that the plasmonic interaction between the phases reduces the amount of heat released respect to a mixed colloid.

Physical Chemistry Chemical Physics Accepted Manuscript

Please do not adjust margins

Conflicts of interest

In accordance with our policy on Conflicts of interest please ensure that a conflicts of interest statement is included in your manuscript here. Please note that this statement is required for all submitted manuscripts. If no conflicts exist, please state that "There are no conflicts to declare".

Acknowledgements

The authors would like to thank the Dr. Ueslen Silva and Prof. Daniel Jaque for their help with the initial test of these systems. This work was supported by the Spanish Ministry of Science and Innovation: MAT2015-67557-C2-2-P and MAT2015-67557-C1-2-P. Financial support from COST Action TD1402 RADIOMAG for a STSM at LPCNO, Tolouse, is also acknowledged.

Notes and references

1 C. M. Cobley, L. Au, J. Chen and Y. Xia, *Expert Opin Drug Deliv*, 2010, **7**, 577–587.
2 J. R. Adleman, D. A. Boyd, D. G. Goodwin and D. Psaltis, *Nano Lett.*, 2009, **9**, 4417–4423.
3 P. D. Dongare, A. Alabastri, S. Pedersen, K. R. Zodrow, N. J. Hogan, O. Neumann, J. Wu, T. Wang, A. Deshmukh, M. Elimelech, Q. Li, P. Nordlander and N. J. Halas, *Proc. Natl. Acad. Sci. U. S. A.*, 2017, **114**, 6936–6941.
4 R. Di Corato, A. Espinosa, L. Lartigue, M. Tharaud, S. Chat, T. Pellegrino, C. Ménager, F. Gazeau and C. Wilhelm, *Biomaterials*, 2014, **35**, 6400–6411.
5 J. R. Melamed, R. S. Edelstein and E. S. Day, *ACS Nano*, 2015, **9**, 6–11.
6 E. A. Périgo, G. Hemery, O. Sandre, D. Ortega, E. Garaio, F. Plazaola and F. J. Teran, *Appl. Phys. Rev.*, 2015, **2**, 041302.
7 D. Jaque, L. Martínez Maestro, B. del Rosal, P. Haro-Gonzalez, A. Benayas, J. L. Plaza, E. Martín Rodríguez and J. García Solé, *Nanoscale*, 2014, **6**, 9494–530.
8 E. C. Abenojar, S. Wickramasinghe, J. Bas-Concepcion and A. C. S. Samia, *Prog. Nat. Sci. Mater. Int.*, 2016, **26**, 440–448.
9 P. Tartaj, M. Del, P. Morales, S. Veintemillas-Verdaguer, T. González-Carr and C. J. Serna, *J. Phys. D Appl. Phys*, 2003, **36**, 182–197.
10 D. Serantes, K. Simeonidis, M. Angelakeris, O. Chubykalo-Fesenko, M. Marciello, M. del P. Morales, D. Baldomir and C. Martinez-Boubeta, *J. Phys. Chem. C*, 2014, **118**, 5927–5934.
11 I. Andreu, E. Natividad, L. Solozábal and O. Roubeau, *ACS Nano*, 2015, **9**, 1408–1419.
12 D. Serantes, D. Baldomir, C. Martinez-Boubeta, K. Simeonidis, M. Angelakeris, E. Natividad, M. Castro, A. Mediano, D.-X. Chen, A. Sanchez, L. Balcells and B. Martínez, *J. Appl. Phys.*, 2010, **108**, 073918.
13 C. Munoz-Menendez, D. Serantes, J. M. Ruso and D. Baldomir, *Phys. Chem. Chem. Phys.*, 2017, **19**, 14527–14532.
14 X. Huang, P. K. Jain, I. H. El-Sayed and M. A. El-Sayed, *Lasers Med. Sci.*, 2008, **23**, 217–228.
15 Y. Bayazitoglu, S. Kheradmand and T. K. Tullius, *Int. J. Heat Mass Transf.*, 2013, **67**, 469–486.
16 M. Grzelczak, J. Perez-Juste, P. Mulvaney and L. M. Liz-Marzan, *Chem Soc Rev*, 2008, **37**, 1783–1791.
17 L. M. Maestro, E. Camarillo, J. A. Sánchez-Gil, R. Rodríguez-Oliveros, J. Ramiro-Bargueño, a. J. Caamaño, F. Jaque, J. G. Solé and D. Jaque, *RSC Adv.*, 2014, **4**, 54122–54129.
18 A. Espinosa, M. Bugnet, G. Radtke, S. Neveu, G. A. Botton, C. Wilhelm, A. Abou-Hassan, V. Budach, A. Jordan, P. Wust, R. Bazzi and E. Pereira, *Nanoscale*, 2015, **7**, 18872–18877.
19 A. Espinosa, R. Di Corato, J. Kolosnjaj-Tabi, P. Flaud, T. Pellegrino and C. Wilhelm, *ACS Nano*, 2016, **10**, 2436–2446.
20 Y. M. Zhou, H. B. Wang, M. Gong, Z. Y. Sun, K. Cheng, X. kai Kong, Z. Guo, Q. W. Chen, M. Zhang, M. H. Cho and T. Hyeon, *Dalt. Trans.*, 2013, **42**, 9906.
21 L. Huang, L. Ao, D. Hu, W. Wang, Z. Sheng and W. Su, *Chem. Mater.*, 2016, **28**, 5896–5904.
22 S. Bhana, G. Lin, L. Wang, H. Starring, S. R. Mishra, G. Liu and X. Huang, *ACS Appl. Mater. Interfaces*, 2015, **7**, 11637–11647.
23 K. C.-F. Leung, S. Xuan, X. Zhu, D. Wang, C.-P. Chak, S.-F. Lee, W. K.-W. K.-W. Ho and B. C.-T. C.-T. Chung, *Chem. Soc. Rev.*, 2012, **41**, 1911.
24 F. Fajaroh, H. Setyawan, A. Nur and I. W. Lenggoro, *Adv. Powder Technol.*, 2013, **24**, 507–511.
25 G. A. Sotiriou, A. M. Hirt, P. Y. Lozach, A. Teleki, F. Krumeich and S. E. Pratsinis, *Chem. Mater.*, 2011, **23**, 1985–1992.
26 J. G. Ovejero, S. J. Yoon, J. Li, A. Mayoral, X. Gao, M. O'Donnell, M. A. García, P. Herrasti and A. Hernando, *Microchim. Acta*, 2018, **185**, 130.
27 B. Nikoobakht and M. A. El-sayed, *Chem. Mater.*, 2003, **15**, 1957–1962.
28 W. Stöber, A. Fink and E. Bohn, *J. Colloid Interface Sci.*, 1968, **26**, 62–69.
29 V. Connord, B. Mehdaoui, R. P. Tan, J. Carrey and M. Respaud, *Rev. Sci. Instrum.*, , DOI:10.1063/1.4895656.
30 U. Kreibig and M. Vollmer, 1995, vol. 25.
31 Y. Davletshin, *MSc Thesis*.
32 E. R. Leite, F. L. Souza, P. R. Bueno, S. de Lazaro and E. Longo, *Chem. Mater.*, 2005, **17**, 4561–4563.
33 J. Carrey and N. Hallali, *Phys. Rev. B* , 2016, **94**, 184420.
34 P. B. Johnson and R. W. Christy, *Phys. Rev. B*, 1972, 6, 4370–4379.
35 M. R. Querry, *Contract. Rep.*, 1985, **CRDC**-**CR**, 85034.
36 E. Palik, Elsevier, 1985.
37 R. Ahijado-Guzmán, G. González-Rubio, J. G. Izquierdo, L. Bañares, I. López-Montero, A. Calzado-Martín, M. Calleja, G. Tardajos and A. Guerrero-Martínez, *ACS Omega*, 2016, **1**, 388–395.
38 R. E. Rosensweig, *J. Magn. Magn. Mater.*, 2002, **252**, 370–374.
39 J. Carrey, B. Mehdaoui and M. Respaud, *J. Appl. Phys.*, 2011, **109**, 083921.
40 M. E. Sadat, K. Baghbador, A. W. Dunn, H. P. Wagner, R. C.

View Article Online DOI: 10.1039/C8CP02517D

Published on 24 August 2018. Downloaded by Freie Universitaet Berlin on 8/24/2018 4:31:16 PM.

Physical Chemistry Chemical Physics Accepted Manuscript

This journal is © The Royal Society of Chemistry 20xx

Please do not adjust margins

Journal Name ARTICLE

View Article Online
DOI: 10.1039/C8CP02513D

Ewing, J. Zhang, H. Xu, G. M. Pauletti, D. B. Mast and D. Shi, *Cit. Appl. Phys. Lett*, 2014, **105**, 91903.

41 M. Rivero, J. Hu, D. Jaque, M. Can, J. Sa and A. Mun, , DOI:10.1021/acs.jpcc.8b03709.

Published on 24 August 2018. Downloaded by Freie Universitaet Berlin on 8/24/2018 4:31:16 PM.

Physical Chemistry Chemical Physics Accepted Manuscript

Please do not adjust margins

View Article Online
DOI: 10.1039/C8CP02513D

Published on 24 August 2018. Downloaded by Freie Universitaet Berlin on 8/24/2018 4:31:16 PM.

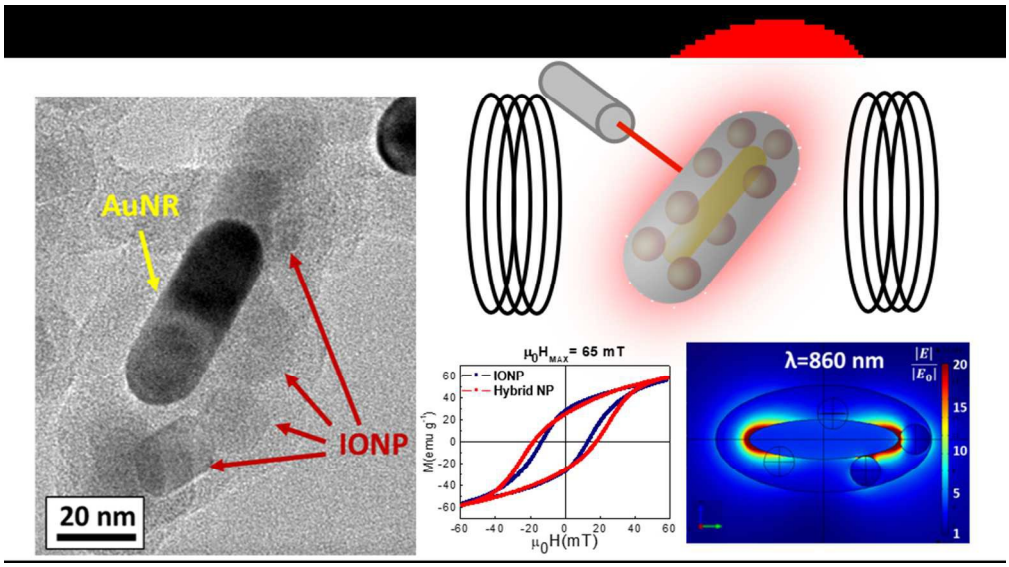

170x94mm (150 x 150 DPI)

Physical Chemistry Chemical Physics Accepted Manuscript